

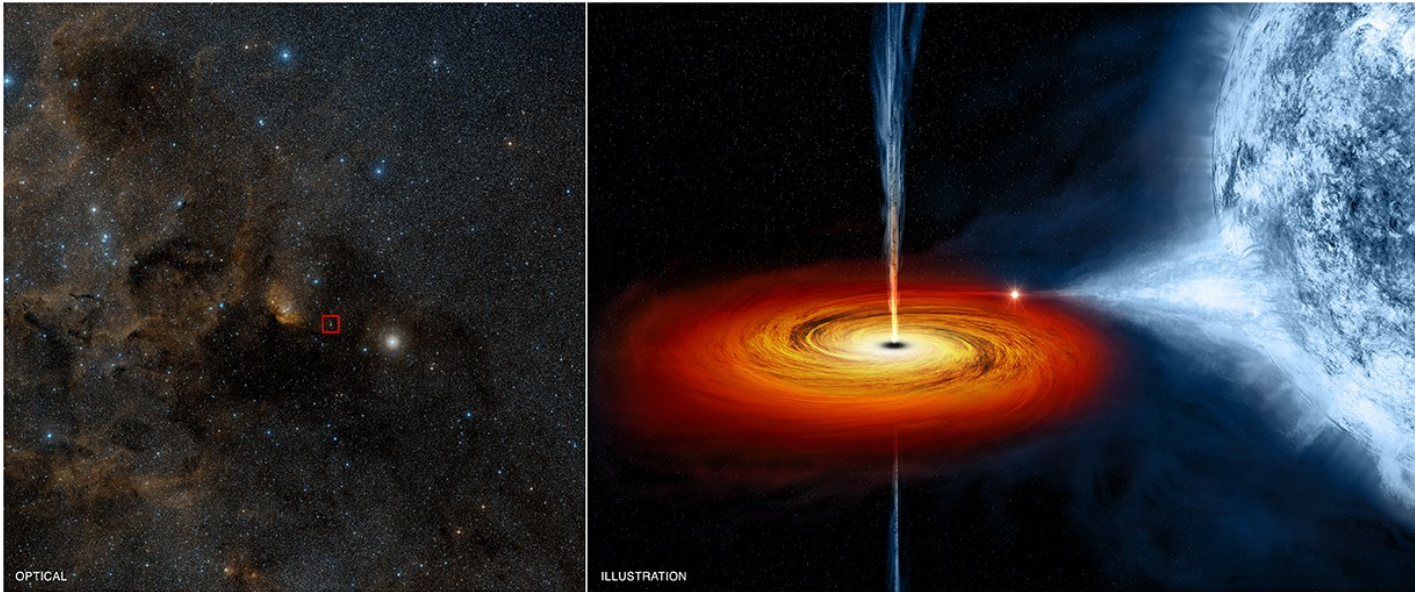
What is the BH spin of Cygnus X-1?



Agnieszka Janiuk

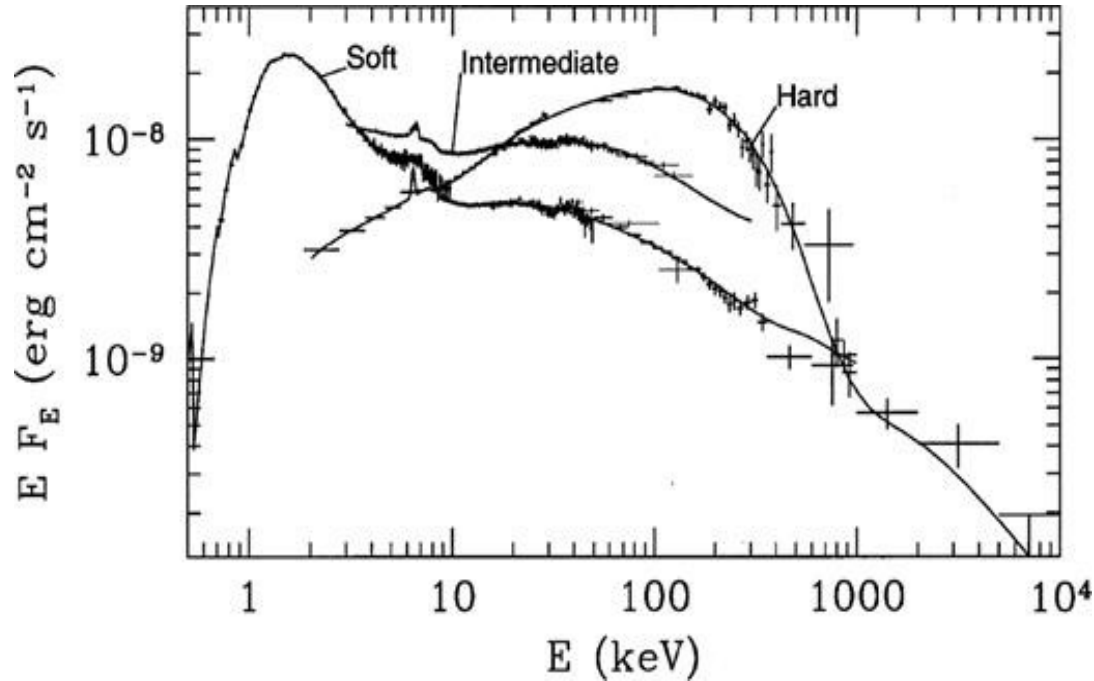
Xth POTOR Conference
17 September 2024

Black Hole in Cygnus X-1



- On the left, an optical image from the Digitized Sky Survey shows Cygnus X-1, outlined in a red box
- Cygnus X-1 is located near large active regions of star formation in the Milky Way, as seen in this image that spans some 700 light years across.
- An artist's illustration is on the right.

State transitions of Cygnus X-1



- Spectra composed of disk black body component and power-law tail
- Hard X-rays possibly originate in a separate medium, i.e. Corona above the disk

Gierliński et al. 1997

High Mass X-ray Binaries



They are progenitors of BBH systems.

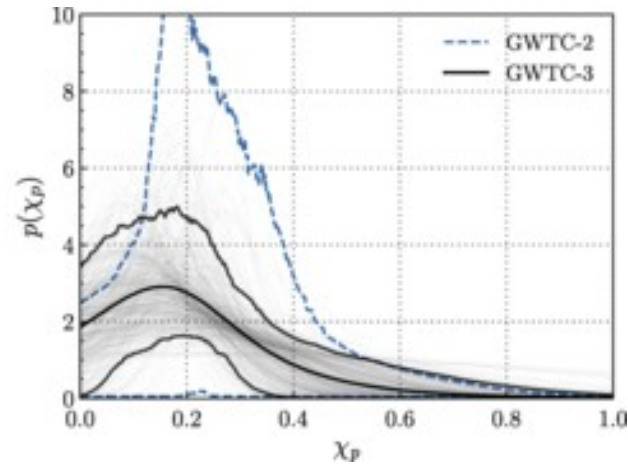
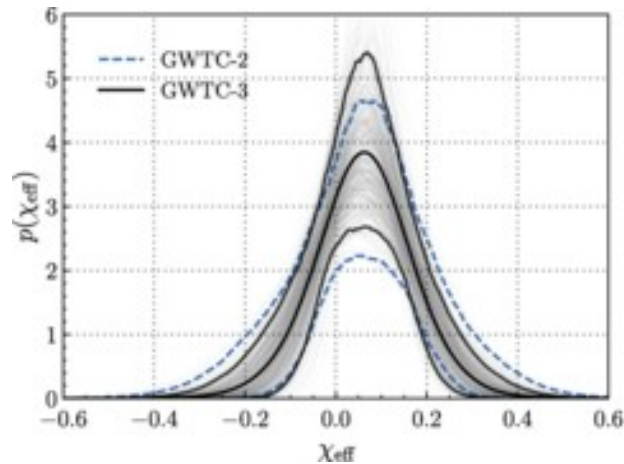
- **Their high spins are in contradiction with LIGO measurements**
- **if these spins are natal**

- BH X-ray binaries (XRBs) with high-mass donors
- Cygnus X-1 (Kerr BH with $a > 0.9985$; Zhao et al. 2021),
- LMC X-1 $a = 0.92^{+0.05}_{-0.07}$ (Gou et al. 2009)
- M33 X-7 $a = 0.84 \pm 0.05$ (Liu et al. 2008)

Spins of Black Holes in binaries: LIGO measurements



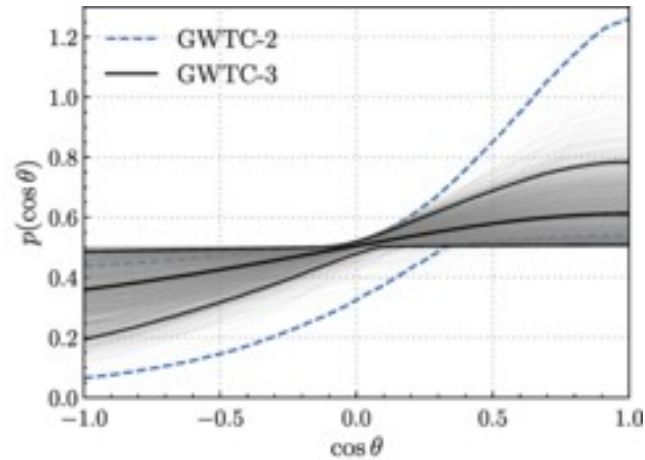
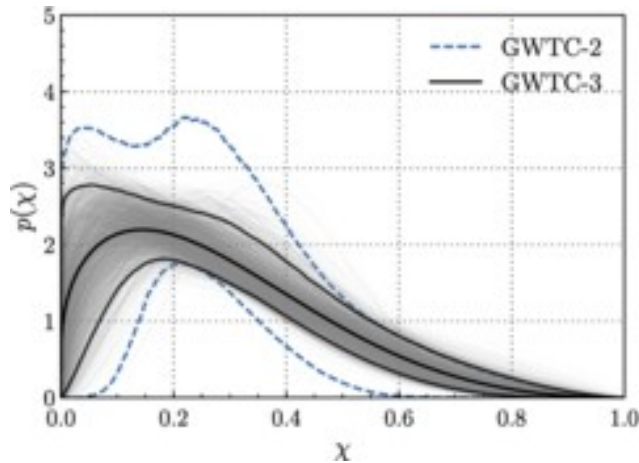
- Spins of merging binary black holes (BBHs) are generally low.
- The most recent population study of Abbott et al. (2023) presents the results from 70 binary BH mergers.
- The effective spin parameter, has the mean value of ≈ 0.06 , and it was < 0.6 in the sample.



Spins of Black Holes in binaries: LIGO measurements



- The distribution of the individual spins peaks at a $\chi_* \approx 0.13^{+0.12}_{-0.11}$, and most of them are $\lesssim 0.4$.

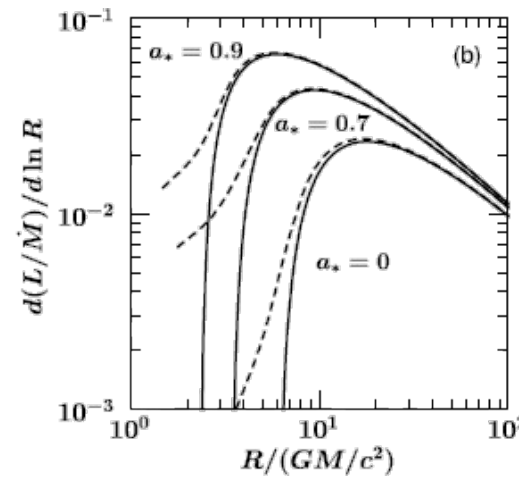
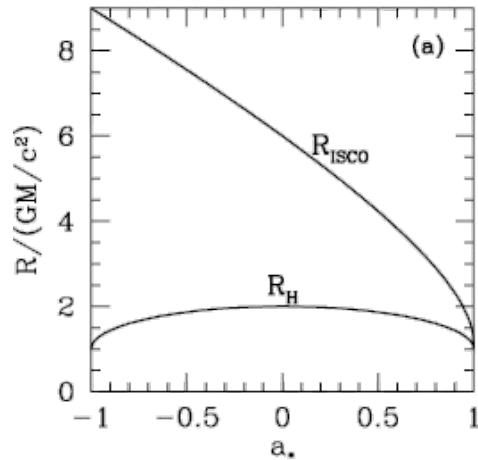


Spin of Black Holes: constraints from X-ray data



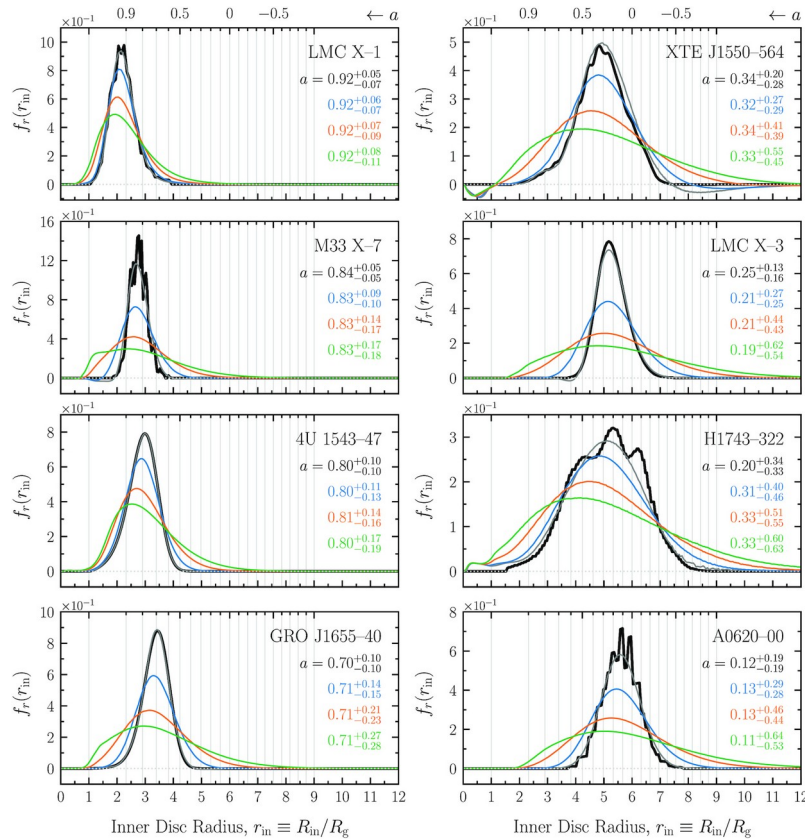
- The method used for the spin determination of the three BH XRBs with high-mass donors was the continuum method, based on fitting the shape of the disk continuum in the soft spectral state (McClintock et al. 2014), knowing the BH mass and distance.
- Major assumption of the continuum model is that the disk is described by the standard accretion model (Novikov & Thorne 1973); disk is extending to ISCO.
- High-energy tails, commonly appearing beyond the disk spectra, are attributed to Comptonization of the disk photons in a corona above the disk.

Spins of Black Holes: constraints from X-ray data

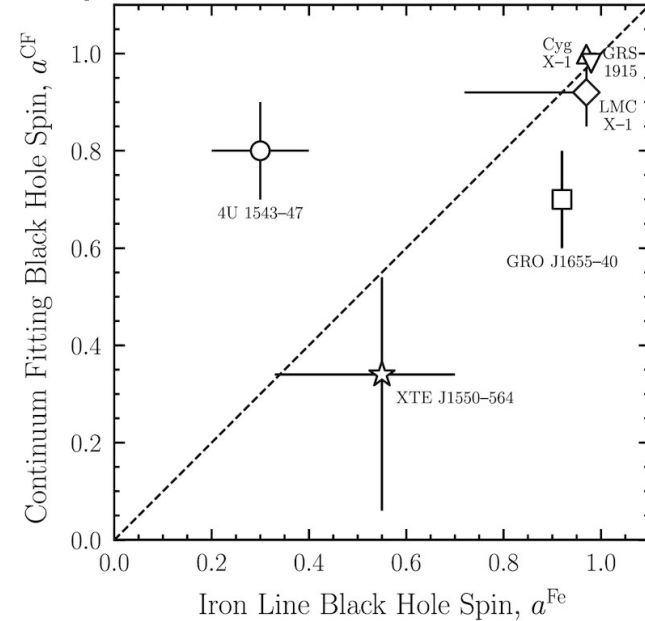


- a) Radius of the ISCO and of the horizon in units of GM/c^2 plotted as a function of the black hole spin parameter a .
- Negative values of a correspond to retrograde orbits.
- (b) Profiles of the differential disk luminosity per logarithmic radius interval normalized by the mass accretion rate, versus radius $R/(GM/c^2)$ for three values of a .
- Solid lines are the predictions of the NT model.

Spins of Black Holes: Constraints from X-ray data



- X-ray Continuum fitting (Salvesen & Miller, 2020)



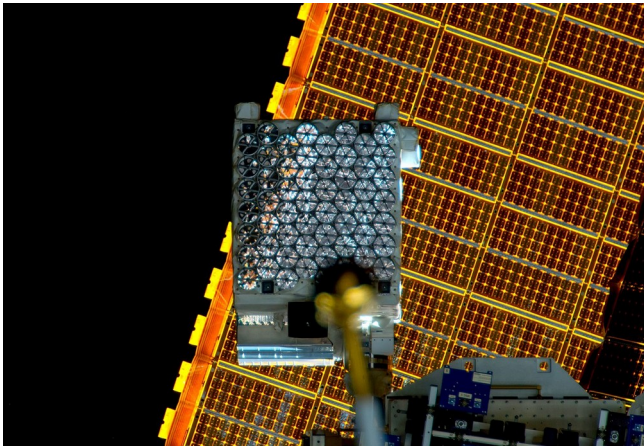
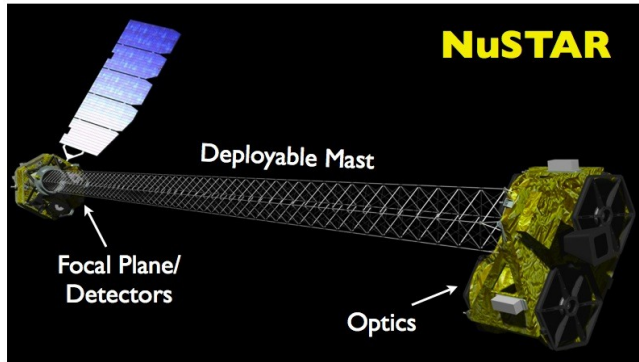
- Iron K-alpha line constraints

Problems with standard accretion disk model



- Unstable due to **radiation pressure**. Emission of Cygnus X-1 in soft state is stable
- Value of **alpha viscosity** is uncertain. Observationally, low-mass BH XRBs show $\alpha \simeq 0.2-1$ (Tetarenko et al. 2018), while local simulations of the standard disk give $\alpha \sim 0.01$ (e.g., Davis et al. 2010; Simon et al. 2011).
- In AGNs, the standard model predicts disk **gravitational fragmentation**, contrary to observations (e.g., Begelman & Pringle 2007).
- Also, AGN **variability time scales** are often much shorter than those for standard disks (e.g., Lawrence 2018).
- The disk sizes inferred from **microlensing** are larger by a factor of a few than those predicted by standard disk theory, e.g., Chartas et al. (2016).

New X-ray observations



- NuSTAR, launched on June 2012 observes in 3-79 keV energy band, with temporal resolution of micro-s
- NICER launched in 2017 is an X-ray observatory that studies neutron stars, black holes, and other phenomena from its home aboard the International Space Station. Energy band 0.2-12 keV
- INTEGRAL: launched by ESA in 2002. Observes sky in energies up to 8 MeV

Cygnus X-1 X-ray data analysis



- The INTEGRAL observation started about 1.4 d after the end of the NICER and NuSTAR ones.
- All observations were clearly in the soft state, and the variability of the 15–50 keV flux during them was modest.

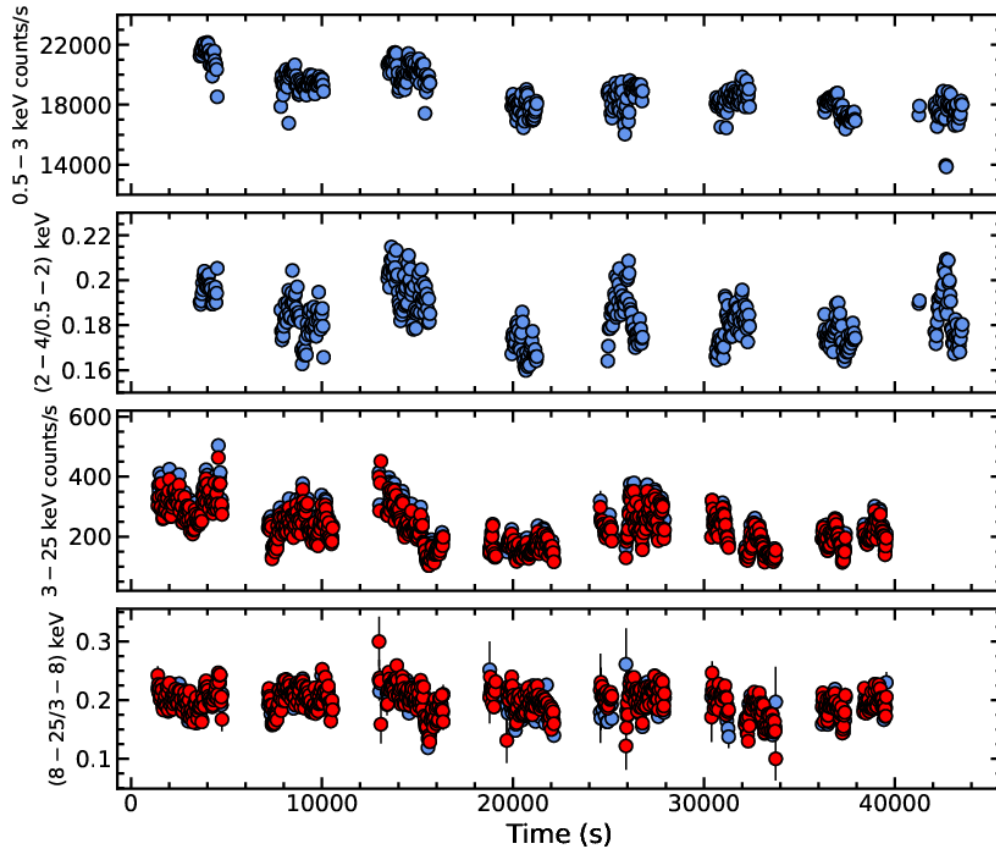
Table 1. Simultaneous observations of Cyg X-1 in the soft state with NICER and *NuSTAR*

Date	Date [MJD]
2018-04-15	58223
2018-05-27	58265
2018-08-11	58341
2019-11-13	58800
2023-05-25	60089
2023-06-20	60115

NOTE—The observation with the weakest high-energy tail, studied here, is marked in bold.

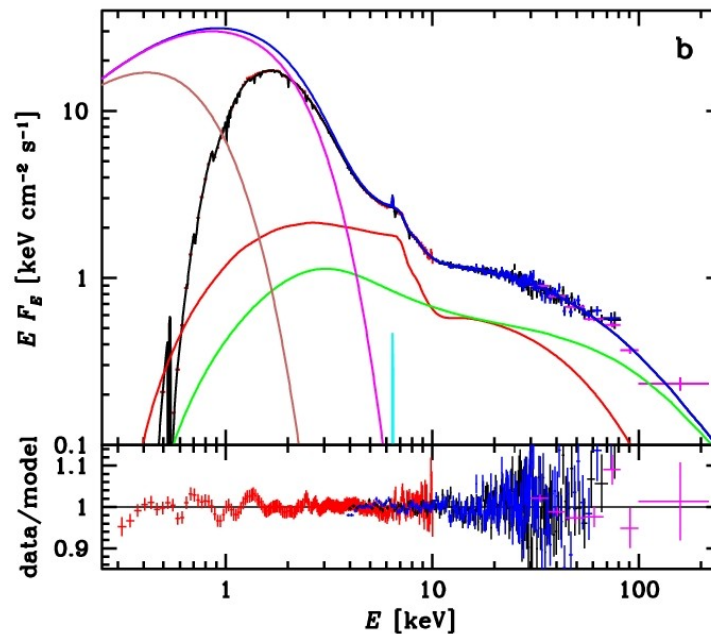
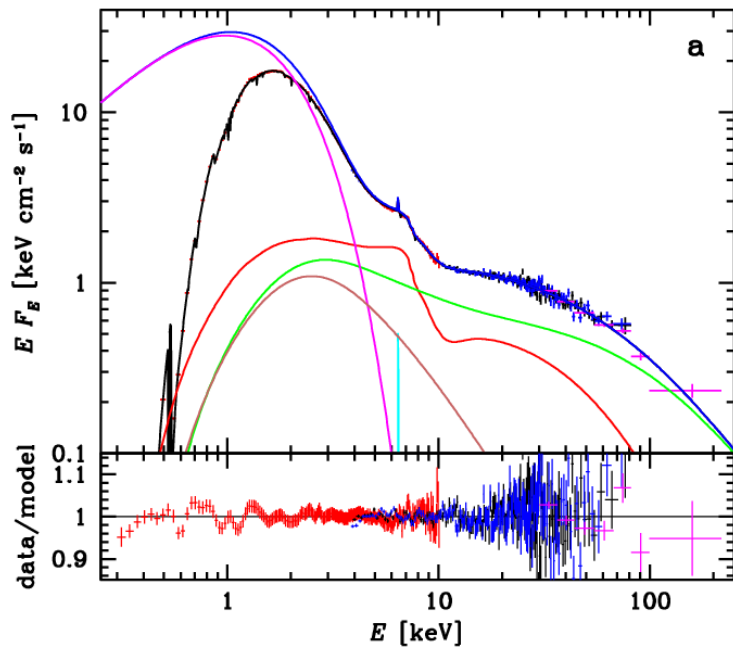
OBS ID's (Zdziarski et al. 2024)

NuSTAR and NICER lightcurves



- Data show the count rates and hardness ratios of NICER and NuSTAR.
- The top two panels show the NICER 0.5–3.0 keV count-rate and the (2–4 keV)/(0.5–2.0 keV) count rate ratio.
- The bottom two panels show the NuSTAR 3–25 keV count-rate and the (8–25 keV)/(3–8 keV) count rate ratio.
- The blue and red symbols correspond to the NuSTAR A and B units, respectively. The zero time corresponds to MJD 58800.42093.
- We see only moderate changes of the count rates and the hardness ratios.

Best fitted spectra



The NICER (red), NuSTAR (black and blue) and INTEGRAL (magenta) unfolded spectra (top panel) and data-to-model ratios (bottom panel) for (a) Model 1 and (b) Model 4.

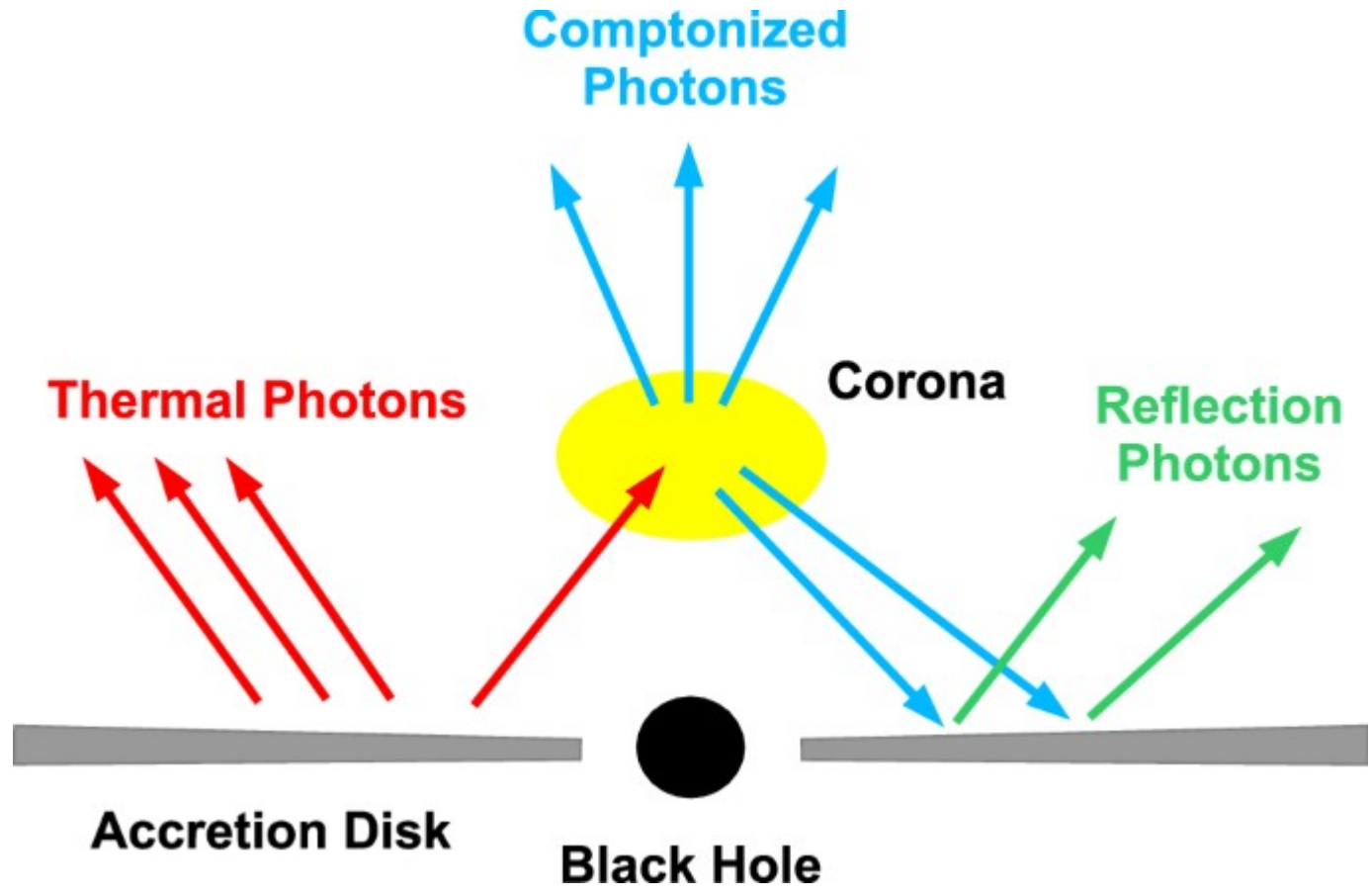
Total model spectrum and the unabsorbed one are shown by the solid black and blue curves, respectively. The unabsorbed disk, scattered, reflected, and narrow Fe K α components are shown by the magenta, green, red and cyan curves, respectively. In (a), the brown curve shows the disk spectrum scattered by the thermal electron component of the hybrid distribution, and in (b), it shows the underlying disk spectrum before going through the Comptonization top layer.

Binary parameters and absorption in Cyg X-1



- Binary inclination is $i_b = 27.5^{+0.8}_{-0.6}$, the mass of the BH is $M_{\text{BH}} = 21.2 \pm 2.2 M_{\odot}$ and the distance to the source is $D = 2.22 \pm 0.18$ kpc (given here as the median values with 68% uncertainties; Miller-Jones et al. 2021).
- The Galactic column density in the direction of Cyg X-1 is $\approx 7.1 \times 10^{21} \text{ cm}^{-2}$ (HI4PI Collaboration et al. 2016)
- Absorption by the stellar wind is modeled by table model of an ionized absorber based on the XSTAR code (Kallman & Bautista 2001) with solar abundances, the H number density of 10^{12} cm^{-3} and the turbulent velocity of 300 km s^{-1} . Its parameters are the ionization parameter, ξ_w , and the column density, N_{H_w} , defined in the ranges of $10^2 \leq \xi_w \leq 10^5 \text{ erg cm s}^{-1}$ and $1 \times 10^{21} \leq N_{\text{H}_w} \leq 5 \times 10^{22} \text{ cm}^{-2}$, respectively.

Geometry sketch



Spectral Models used



Table 3. The results of spectral fitting

Component	Parameter	Model 1	Model 2	Model 3	Model 4	
Absorption	N_{H} [10^{21} cm^{-2}]	$7.23^{+0.04}_{-0.04}$	$7.16^{+0.04}_{-0.04}$	$7.20^{+0.04}_{-0.04}$	$7.53^{+0.19}_{-0.09}$	
	Z_{O}	$1.09^{+0.02}_{-0.02}$	$1.08^{+0.02}_{-0.02}$	$1.09^{+0.02}_{-0.02}$	$1.10^{+0.02}_{-0.02}$	
	Z_{Fe}	$0.50^{+0.03}_{-0.03}$	$0.50^{+0.02}_{-0.02}$	$0.50^{+0.07}_{-0.07}$	$0.50^{+0.04}_{-0.04}$	
	$N_{\text{H,wind}}$ [10^{21} cm^{-2}]	$2.0^{+0.8}_{-0.4}$	$3.6^{+0.6}_{-0.9}$	$3.6^{+0.6}_{-0.9}$	$3.4^{+0.5}_{-1.0}$	
	$\log_{10}(\xi_{\text{wind}})$	$3.66^{+0.06}_{-0.08}$	$3.80^{+0.07}_{-0.07}$	$3.78^{+0.07}_{-0.06}$	$3.77^{+0.06}_{-0.14}$	
Disk	a_*	$0.88^{+0.04}_{-0.01}$	$0.92^{+0.07}_{-0.05}$	$0.985^{+0.006}_{-0.004}$	$0.04^{+0.26}_{-0.04}$	
	i [$^\circ$]	40^{+1}_{-1}	27.5f	27.5f	38^{+1}_{-1}	
	f_{col}	$1.73^{+0.06}_{-0.05}$	$1.90^{+0.05}_{-0.22}$	1.7f	$1.22^{+0.44}_{-0.03}$	
	\dot{M}_{disk} [10^{18} g s^{-1}]	$0.35^{+0.01}_{-0.04}$	$0.30^{+0.01}_{-0.01}$	$0.24^{+0.01}_{-0.01}$	$0.44^{+0.04}_{-0.04}$	
Coronal	$\ell_{\text{h}}/\ell_{\text{c}}$	$0.31^{+0.01}_{-0.11}$	$0.40^{+0.10}_{-0.05}$	$0.46^{+0.03}_{-0.02}$	$0.64^{+0.12}_{-0.10}$	
	$\ell_{\text{nth}}/\ell_{\text{h}}$	$0.62^{+0.20}_{-0.02}$	$0.64^{+0.01}_{-0.01}$	$0.61^{+0.01}_{-0.01}$	$0.92^{+0.08}_{-0.11}$	
Comptonization	τ_{T}	$0.18^{+0.09}_{-0.02}$	$0.28^{+0.12}_{-0.01}$	$0.33^{+0.14}_{-0.01}$	$0.75^{+0.71}_{-0.09}$	
	Γ_{inj}	$0.2^{+0.3}_{-0.2}$	$0^{+0.1}_{-0.1}$	$0^{+0.1}_{-0.1}$	$0.7^{+0.1}_{-0.4}$	
	γ_{max}	$6.5^{+0.5}_{-0.5}$	$6.5^{+0.4}_{-0.9}$	$6.5^{+0.4}_{-0.5}$	$6.0^{+0.1}_{-0.4}$	
	f_{cov}	$0.18^{+0.01}_{-0.05}$	$0.11^{+0.01}_{-0.01}$	$0.09^{+0.01}_{-0.01}$	$0.07^{+0.01}_{-0.01}$	
	kT_{e} [keV]	61	51	48	33	
	Disk skin	τ_{T}	–	–	–	31^{+2}_{-1}
	Comptonization	kT_{e} [keV]	–	–	–	$0.44^{+0.01}_{-0.01}$
Reflection and	\mathcal{R}	$0.9^{+0.1}_{-0.1}$	$1.2^{+0.1}_{-0.1}$	$1.3^{+0.1}_{-0.1}$	$1.2^{+0.1}_{-0.1}$	
	narrow line	$\log_{10} \xi$	$3.93^{+0.28}_{-0.08}$	$4.26^{+0.06}_{-0.08}$	$4.25^{+0.08}_{-0.06}$	$4.08^{+0.15}_{-0.06}$
narrow line	β	$3.1^{+0.1}_{-0.3}$	$2.2^{+0.1}_{-0.1}$	$2.2^{+0.1}_{-0.1}$	$5.3^{+1.9}_{-0.8}$	
	Z_{Fe}	$5.3^{+0.5}_{-0.5}$	$6.0^{+0.3}_{-0.3}$	$6.0^{+0.2}_{-0.2}$	$6.0^{+0.4}_{-0.4}$	
	E_{line} [keV]	$6.44^{+0.01}_{-0.04}$	$6.44^{+0.05}_{-0.04}$	$6.44^{+0.05}_{-0.04}$	$6.44^{+0.03}_{-0.04}$	
	N_{line} [$10^{-4} \text{ cm}^{-2} \text{ s}^{-1}$]	$8.5^{+2.1}_{-2.2}$	$6.1^{+2.3}_{-2.0}$	$6.7^{+2.2}_{-1.9}$	$8.4^{+2.2}_{-2.2}$	
	Cross-calibration	$\Delta\Gamma_{\text{NICER}}$	$-0.072^{+0.009}_{-0.009}$	$-0.072^{+0.11}_{-0.01}$	$-0.076^{+0.009}_{-0.005}$	$-0.072^{+0.13}_{-0.08}$
K_{NICER}		$1.00^{+0.01}_{-0.01}$	$1.00^{+0.02}_{-0.01}$	$0.99^{+0.01}_{-0.01}$	$1.00^{+0.02}_{-0.02}$	
K_{NuSTAR}		$0.994^{+0.003}_{-0.004}$	$0.995^{+0.002}_{-0.005}$	$0.993^{+0.004}_{-0.003}$	$0.994^{+0.003}_{-0.004}$	
K_{INTEGRAL}		$1.30^{+0.02}_{-0.02}$	$1.36^{+0.02}_{-0.02}$	$1.30^{+0.02}_{-0.02}$	$1.30^{+0.02}_{-0.02}$	
	χ^2_{ν}	530/607	547/608	547/609	519/605	

NOTE—Models 1, 2 and 3 = `plabs*tbfeo*wind_abs(relconv*xilconv*ceqpair*kerribb + ceqpair*kerribb + kerribb*gaussian)`; Model 4 = `plabs*tbfeo*wind_abs(relconv*xilconv*ceqpair*thcomp*kerribb + ceqpair*thcomp*kerribb + thcomp*kerribb*gaussian)`. The four additive components represent the reflection of the scattered radiation, the scattered emission going to the observer, the unscattered disk emission and the narrow line from distant fluorescence. In coronal Comptonization, kT_{e} is the best fit value (not a free parameter), $\xi \equiv 4\pi F_{\text{irr}}/n$ is the ionization parameter, where F_{irr} is the irradiating flux. We have constrained $a_* \geq 0$, $Z_{\text{Fe}} \geq 0.5$ and ≤ 6 for the Galactic absorption and reflection, respectively, $\Gamma_{\text{inj}} \geq 0$, and $6.4 \text{ keV} \leq E_{\text{Fe}} \leq 7.0 \text{ keV}$.

- **Eqpair model for Compton scattering**, treats $e\pm$ pair production/annihilation, bremsstrahlung, and energy exchange between thermal and non-thermal parts of the electron distribution by Coulomb scattering. (Poutanen & Coppi 1998)
- Some of electrons are accelerated, and the thermal ones are heated. The resulting non-thermal part of the distribution and the electron temperature, kT_{e} , are calculated self-consistently.
- Covering of the disk by a **warm scattering layer** with $kT_{\text{e}} \sim 1 \text{ keV}$ and $\tau_{\text{T}} \gg 1$. Modeled by the *thcomp* code (Zdziarski 2020)
- **Relativistic reflection/reprocessing** features, using the convolution model, *xilconv*, based on the *relxill* opacity tables of García et al. (2013) and the Green's functions of Magdziarz & Zdziarski (1995). The reflection features are then relativistically broadened, by model *relconv* (Dauser et al. 2010). It assumes a power-law radial distribution of the irradiation, $\propto R^{-\beta}$, with β to be a free parameter.

Discussion: spin model dependence



- The value of $a > 0.9985$ obtained by Zhao et al. (2021) and Miller-Jones et al. (2021) is beyond theoretical limit of $a = 0.998$ (Thorne 1974).
- This result can be reconciled with **our fit (Model 3) to $a = 0.985$** , with inclination 27.5 and $f_{\text{col}} = 1.7$, once relativistically broadened reflection is included.
- Relaxing the color correction and fit with $f_{\text{col}} = 1.9$, **(Model 2) reduces BH spin to $a = 0.92$** . Color correction may be different due to presence of large scale magnetic fields.
- Relaxing inclination to $i = 40$, gives **$a = 0.88$ (Model 1)**, with $f_{\text{col}} = 1.7$ – inner disk inclination may be different from binary's
- **Non standard Model 4** with optically thick Comptonizing layer gives much better fit (in terms of χ^2) but yields extremely small spin value **$a = 0.04$** . It is motivated by analogy with Soft Excess in AGN. Reflection broadening is compensated by steep irradiation power-law index, in case of small spin.

Discussion: jet models and spin



- There are two main jet models for accreting BHs: **BZ-77** and **BP-82**. In both, the jet formation requires a poloidal magnetic field.
- Highest jet power obtained from GR MHD simulations relates it with magnetic flux at horizon and BH spin, $P_{j,\max} \approx 1.3 \dot{M}_{\text{accr}} c^2 a^2$
- Values of $a \ll 1$ for the three known high-mass BH XRBs are not in conflict with the jet observations. LMC X-3 and M33 X-7 have no jets. **Cyg X-1 has a prominent compact jet**, but its estimated power is **consistent with** $\ll \dot{M}_{\text{accr}} c^2$
- Transient jets during hard-to-soft state transitions have been observed from about 15 low-mass BH XRBs. Their propagation through the surrounding cavities and the ISM requires, at least in some cases, their power to be $\sim \dot{M}_{\text{accr}} c^2$, hence $a \sim 1$.

Spin-up by accretion



$$a_1 = \frac{r_{\text{ISCO}}(a_0)^{\frac{1}{2}}}{3M/M_0} \left\{ 4 - \left[\frac{3r_{\text{ISCO}}(a_0)}{(M/M_0)^2} - 2 \right]^{\frac{1}{2}} \right\},$$

$$\frac{M}{M_0} = \left[\frac{3r_{\text{ISCO}}(a_0)}{2} - 1 \right]^{\frac{1}{2}} \sin \left\{ \left[\frac{2}{3r_{\text{ISCO}}(a_0)} \right]^{\frac{1}{2}} \frac{\Delta M}{M_0} \right\} \\ + \cos \left\{ \left[\frac{2}{3r_{\text{ISCO}}(a_0)} \right]^{\frac{1}{2}} \frac{\Delta M}{M_0} \right\},$$

$$t_E = \frac{\eta(1 + X)c\sigma_T}{8\pi(1 - \eta)Gm_p},$$

- We made estimate based on Bardeen (1970) formalism is that a fraction of ≈ 0.40 ($\approx 8.5M_\odot$ for the current BH mass of $M=21.2M_\odot$) of the present mass needed to be accreted, **if the spin changed from $a_0=0.1$ to $a_1=0.9$**
- In the Eddington limit, time for accretion to increase the mass from M_0 to M is **$t \sim t_E \ln(M/M_0) \approx 17$ Myr.** (accretion increases mass exponentially, $t_E \sim 34$ Myrs for $X=0.5$, $\eta=0.1$)
- This is much longer than the estimated **lifetime of Cyg X-1 of ~ 4 Myr** (Miller-Jones et al. 2021).

Spin-up by accretion

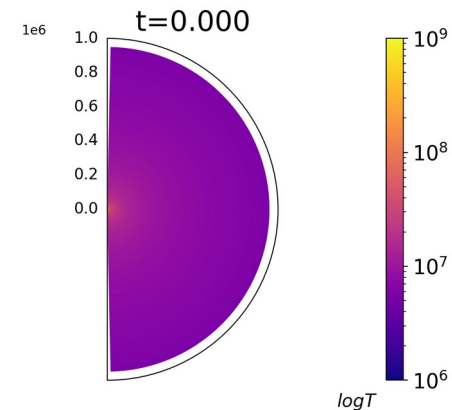
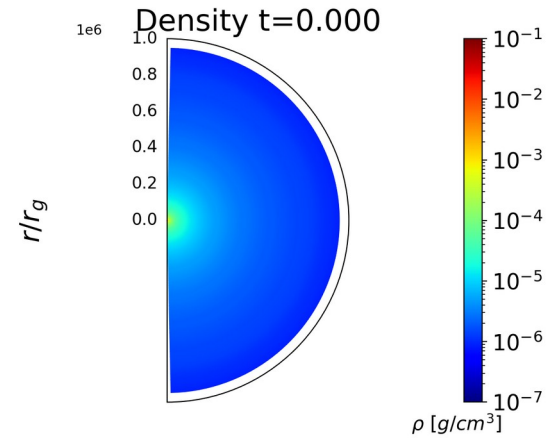


- In our Models 1 and 2, $a \sim 0.9$. For a natal spin, i.e., $a \sim 0.1$, the BH needed to be spun up by accretion from the donor. Eddington limited accretion is excluded though.
- Recently, Qin et al. (2022) assumed super-Eddington accretion in Cyg X-1 and performed study where peak mass transfer rate is $\dot{M} \approx 10^{-2} M_{\odot}/\text{yr} \approx 6 \times 10^{23} \text{ g s}^{-1}$, corresponding to $\dot{M} c^2 \approx 6 \times 10^{44} \text{ erg s}^{-1}$.
- They assumed the accretion is conservative due to the excess accretion energy radiated away via formation of neutrino pairs.

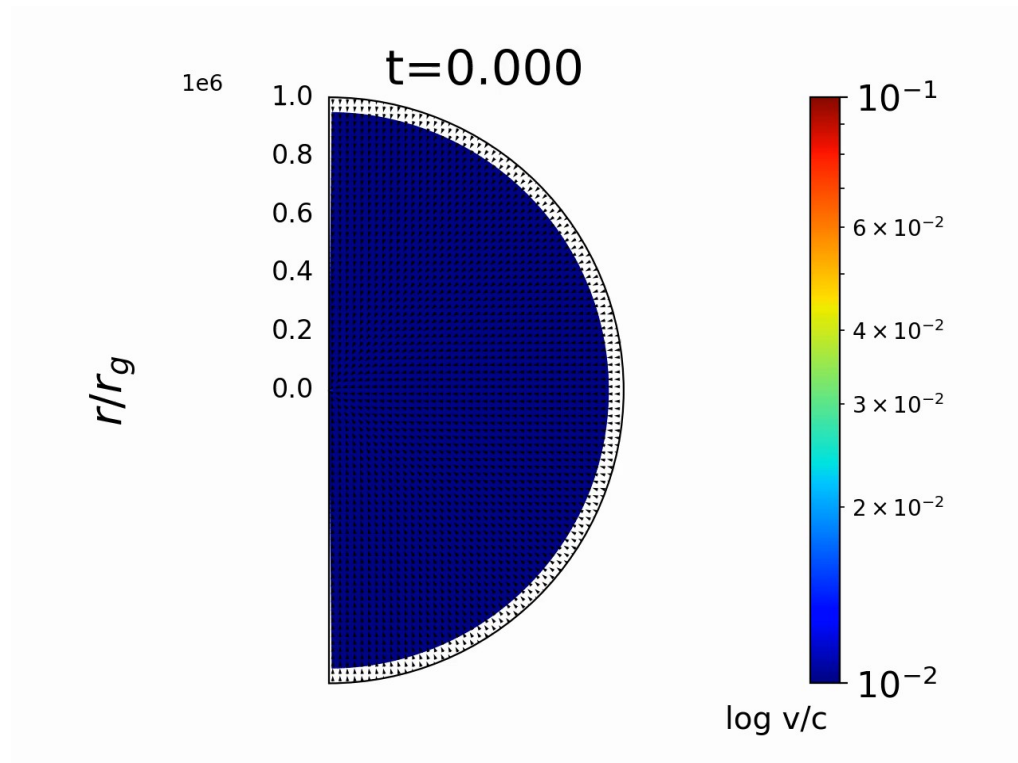
Neutrino-cooled accretion flow



- We have adopted parameters of **super-Eddington accretion** based on analytic model of Poutanen et al. (2007).
- The spherisation radius at the $\dot{M} = 10^{-2} M_{\odot}/\text{yr}$ is $R_{\text{sph}} \approx 3 \times 10^{12}$ cm, and the mass enclosed within it is $\approx 10^{-5} M_{\odot}$.
- We approximated the flow by a quasi-spherical, low angular momentum, supersonic gas, which can be partly cooled by neutrinos.
- Neutrinos are produced mainly by electron-positron pair annihilation (cf. **HARM_COOL; Janiuk 2019**; current code is using the rates of Rosswog & Liebendörfer 2003).



Numerical simulation of neutrino cooled accretion

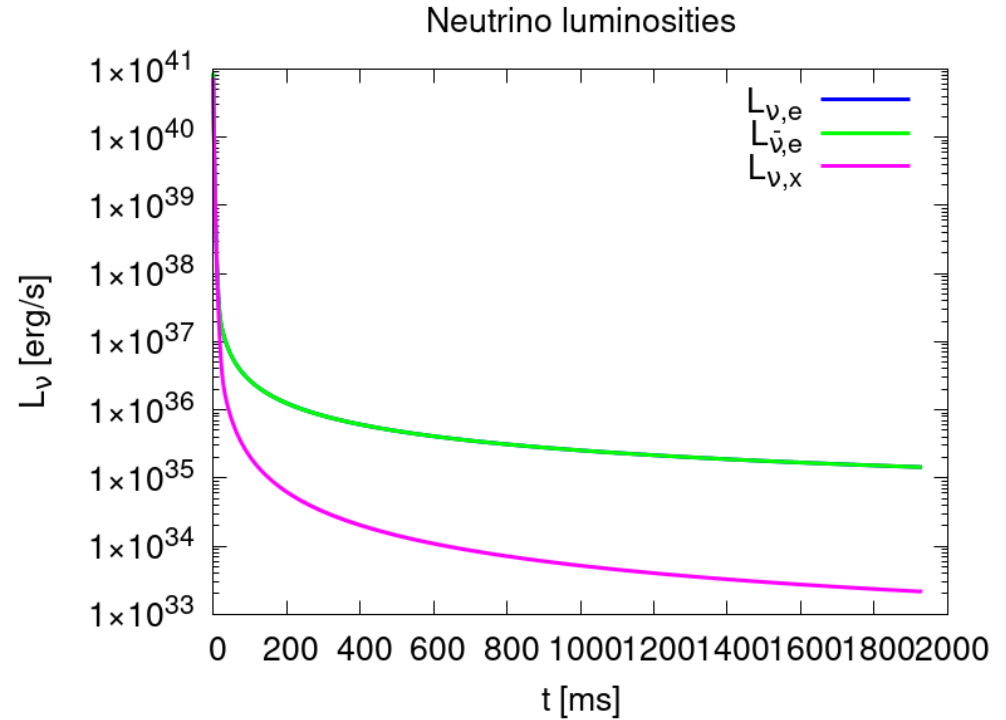


Numerical simulation of neutrino cooled accretion



The heavy lepton neutrinos are negligible due to small density.

Even for electron-antielectron neutrinos, their small luminosities are insufficient to affect system dynamics, with $\dot{M}c^2 \sim 10^{44}$ erg/s



Summary



We have found the measured BH spin parameter of Cyg X-1 to be strongly dependent on the way the disk is modeled.

The best model we have found is that of hybrid Comptonization, which we modeled by a convolution version of *eqpair*, with the seed photons from a relativistic disk, modelled by *kerrbb*.

Our measurements confirm the previous results of $a_* \gtrsim 0.99$.

We consider also the case of the dissipation in a warm surface layer, as motivated by successful modeling of soft X-ray excesses in AGNs.

Then, Comptonization in that layer leads to very low spins, $a_* \approx 0.04$.

This result can resolve the tension between the low BH spins inferred from analyses of merger events detected in gravitational waves and the prevalence of high spins estimated by spectral fitting of BH XRBs.

Conclusions



- Broad-band X-ray data on Cyg X-1 obtained in the soft spectral state by simultaneous NICER and NuSTAR, as well as INTEGRAL observations, were fitted with hybrid Comptonisation model of the 'kerrbb' disk seed photons.
- The spin parameters of the disk and relativistic broadening models were fitted, combining the disk continuum and the reflection spectroscopy methods of spin determination.
- The measured BH spin parameter of Cyg X-1 is strongly dependent on the way the disk is modeled. For standard disk, $a \geq 0.99$ is obtained. For warped disk, and various color corrections resulting from magnetized disk model, we get $a = 0.88-0.92$.
- For the case of the dissipation occurring also in a warm surface layer, as motivated by soft X-ray excesses in AGN, the spin is low, $a = 0.04$.

Bibliography



A. Zdziarski, S. Chand, S. Banerjee, M. Szanecki, A. Janiuk, P. Lubiński, A. Niedźwiecki, G. Dewangan, R. Misra

Astrophysical Journal Letters, 2024, 967, 9

arXiv:2402.12325

What Is the Black Hole Spin in Cyg X-1?

ANDRZEJ A. ZDZIARSKI,¹ SWADESH CHAND,² SRIMANTA BANERJEE,² MICHAŁ SZANECKI,³ AGNIESZKA JANIUK,⁴
PIOTR LUBIŃSKI,⁵ ANDRZEJ NIEDŹWIECKI,³ GULAB DEWANGAN,² AND RANJEEV MISRA²

¹*Nicolaus Copernicus Astronomical Center, Polish Academy of Sciences, Bartycka 18, PL-00-716 Warszawa, Poland; aaz@camk.edu.pl*

²*Inter-University Center for Astronomy and Astrophysics, Pune 411007, India*

³*Faculty of Physics and Applied Informatics, Łódź University, Pomorska 149/153, PL-90-236 Łódź, Poland*

⁴*Center for Theoretical Physics PAS, Al. Lotników 32/46, 02-668 Warsaw, Poland*

⁵*Institute of Physics, University of Zielona Góra, Licealna 9, PL-65-417 Zielona Góra, Poland*